Tribology Letters (2020) 68:130
https://doi.org/10.1007/s11249-020-01377-8

ORIGINAL PAPER

Ionic Liquids as Additives in Water-Based Lubricants: From Surface Adsorption to Tribofilm Formation

H. Khanmohammadi[1] · W. Wijanarko[1] · N. Espallargas[1]

Received: 18 September 2020 / Accepted: 11 November 2020 / Published online: 21 November 2020

Abstract
Ionic liquids (ILs) are potential lubricant additives that can potentially perform simultaneously as friction modifiers and anti-wear agents. In addition, they possess good thermal stability, they are non-flammable, they have high polarity with negligible volatility, etc. These characteristics make them also ideal for polar lubricants, like water-based fluids. In this work, the friction and wear mechanisms of stainless steel 316L tested in water-based lubricants containing three different ionic liquids, i.e. Tributylmethylphosphonium dimethylphosphate, (2-hydroxyethyl) trimethylammonium dimethylphosphate and 1-butyl-1-methylpyrrolidinium tris(pentafluoroethyl)trifluorophosphate, have been investigated and compared with a reference water-based lubricant containing dodecanoic acid (Lauric acid, C12) as a well-known organic friction modifier. All lubricants formulated with the three ionic liquids showed frictional values lower than the water-based lubricant alone, but higher than the lubricant formulated with C12. A detailed surface adsorption study using Quartz Crystal Microbalance with Impedance measurements (QCM-I) revealed differences in the adsorption kinetics, strength of the adsorption bonds to the metallic surface and also different viscoelastic properties of the adsorbed layers for all the different additives. In the case of one of the ionic liquids (1-butyl-1-methylpyrrolidinium tris(pentafluoroethyl)trifluorophosphate), a tribofilm is formed after some sliding cycles and a significant friction to values lower than that of C12 is observed. A detailed surface and sub-surface investigation of the structure and the chemistry of the wear tracks using SEM/FIB, S(T)EM, and XPS showed that an oxide-rich tribolayer built in the wear track was the cause for the decrease in both wear rate and coefficient of friction. The other ionic liquids were not able to create a tribofilm on the surface of the steel and therefore friction and wear values were higher.

Keywords Ionic liquids · Water-based lubricants · Surface adsorption · tribofilm

1 Introduction

Lubricants are chemical products composed of a base stock and various additives designed to fulfil the requirements of a tribo-system [1]. Additives are the most important chemical substances in a lubricant since they are responsible for providing the functionality to the lubricant in terms of friction, wear, oxidation resistance, anti-foaming, etc. The chemistry of additives used in lubricants vary depending on the applications and the market they are targeting. However, the two most important types of additives are typically friction modifiers and anti-wear additives. Classical friction modifiers are Organic Friction Modifiers (OFM), which are typically carboxylic acids of different hydrocarbon length. Classical antiwear additives usually contain reactive atoms such as phosphorus (P), sulphur (S), nitrogen (N) or halogens able to react with the surface forming a protective layer [2, 3]. The most widely used anti-wear additive is ZDDP (Zinc dialkyldithiophosphate), which was originally designed to be an anti-oxidant [4]. However, it was soon found that it had a very good ability to form films on the contacting metallic surfaces which protected them against wear, making it very quickly popular as an anti-wear additive. However, ZDDP is also known for its tendency to generate deposits and ashes due to thermal decomposition that might also contribute to environmental issues [5]. New types of

Electronic supplementary material The online version of this article (https://doi.org/10.1007/s11249-020-01377-8) contains supplementary material, which is available to authorized users.

✉ H. Khanmohammadi
hamid.khanmohammadi@ntnu.no

[1] Norwegian Tribology Centre, Department of Mechanical and Industrial Engineering, Norwegian University of Science and Technology (NTNU), Trondheim, Norway

additives with better performance are always under investigation by both lubricant manufacturers and academia. In the recent years, Ionic Liquids (ILs) are emerging as potential lubricant additives due to their unique physicochemical characteristics and inherent polarity for strong surface adsorption [6].

ILs are known as room temperature molten salts consisting of an anionic and a cationic part. Based on their chemical composition, ILs show some unique properties that can be optimized by the proper combination of the anionic or cationic part; such as low vapour pressure, non-flammability, ash less behaviour, high thermal stability and environmentally friendly properties [7, 8]. ILs have been also broadly studied as base stocks in addition to as additives [2, 9–11]. A significant advantage of using ILs as lubricant additives is that they can potentially provide with multi-functionality to the lubricants acting simultaneously as friction modifier, anti-wear additive and extreme pressure additive [12].

ILs as lubricant additives are only recently investigated and their lubrication mechanisms are still under debate. Two lubrication mechanisms for ILs are proposed in the literature: (1) the formation of adsorbed layers and (2) the tribofilm formation on metal surfaces [13]. *Adsorbed layers* on metal surfaces have low shear strength and facilitate the motion of two sliding surfaces by decreasing the coefficient of friction. It has been suggested that the adsorption mechanism occurs by the attraction of the anionic part of the IL to the positively charged metal surface [13, 14]. Consequently, a multi-layered structure of anions and cations can be formed on the metal surfaces leading to a decrease in friction. Depending on the ionic nature of both anionic and cationic parts of the IL, higher surface adsorption to metallic surfaces can create a thin, soft and brushy adsorbed layer that acts as friction modifier [13–17].

For the second lubricating mechanism, the formation of *tribofilms* on the metal surface would be the result of a tribochemical reaction between the IL and the metal surface [2, 13]. During the process of rubbing of two surfaces, local high temperature can be achieved causing the decomposition of the IL leading to the formation of a tribofilm [13, 18–21]. The in-situ formed tribofilm can lead to decrease in both friction and wear, and this would eventually enable the additive to act simultaneously as friction modifier and anti-wear agent.

This work aims to investigate the lubricating mechanisms of three different ILs in water-based lubricants comparing their functionality with dodecanoic acid (C12), which is a well-known OFM. In this work, it will be investigated whether their ionic nature makes them reactive towards metal surfaces bringing the possibility of creating either adsorbed layers or tribofilms. The lubricating mechanisms are discussed based on the study of the surface adsorption kinetics of the formulated lubricants on QCM sensors coated with stainless steel, and the surface chemical and microstructural analysis of the wear tracks after testing the same lubricants on stainless steel sliding against alumina.

2 Experimental Procedure

2.1 Materials

AISI 316L grade austenitic stainless steel was chosen as the test material. Test samples were cut from a steel rod with a diameter of 25 mm in the shape of disks with the thickness of 6 mm. Specimen surfaces were ground to 4000 grit SiC paper followed by polishing with a suspension consisting of 3 µm diamond particles. The polished samples were cleaned ultrasonically in ethanol for 10 min, subsequently rinsed with fresh ethanol and dried with pressurized air.

The water-based lubricant was prepared with a mixture of 50–50 weight percent of distilled water and a glycol. Three different ionic liquids (Table 1) were added to the water-based lubricant as additives with a concentration of 1 wt% and the reference lubricant was formulated with 0.1 wt% dodecanoic acid. The concentration of dodecanoic acid is ten times smaller than in the lubricants formulated with ILs since in previous works it has been found that this is the optimal concentration for this base lubricant to avoid micelle formation [22]. The ionic structure, chemical formula and molecular weight of the four additives are listed and shown in Table 1. The formulated mixtures were prepared by magnetic stirring at 40 °C for 2 h and then the electrical conductivity and pH of the lubricants were measured by means of a HANNA HI-2300 Benchtop conductivity meter.

2.2 Testing and Characterization Methods

The dynamic viscosity of the formulated lubricants was measured by means of a Haake Mars Rotational Rheometer at 23 °C in humid air. The shear rate was increased from 0.01 to 500 s^{-1}, held at a constant shear rate of 500 s^{-1} for 30 s and then decreased to the initial value. The mentioned cycle was repeated twice for each lubricant and the average value of 60 measurements at the constant shear rate is reported as the viscosity number. The density of lubricants was measured by weighing the constant volume of the fluids. Table 2 summarizes the viscosity, density, electric conductivity and pH of the formulated water-based lubricants and the open circuit potential (OCP) of the 316L stainless steel samples in the formulated lubricants before starting the wear tests.

The adsorption studies were performed using a *Quartz crystal microbalance with impedance measurement (QCM-I)* supplied by MicroVacuum Ltd. (Budapest, Hungary). The resonance sensitivity of the instrument in liquid is 0.2 Hz, the dissipation sensitivity is 1×10^{-7} and the mass sensitivity

Table 1 Chemical formula, molecular weight and chemical structure of the additives used in this study

Additive's acronym	Chemical name	Chemical formula	Molecular weight (g/mol)	Density (g/cm^3)	Chemical structure
AM	(2-hydroxyethyl) trimethylammonium dimethylphosphate	$C_7H_{20}NO_5P$	229.21	1.186	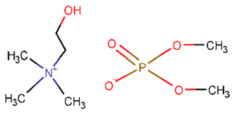
PP	Tributylmethylphosphonium dimethylphosphate	$C_{15}H_{36}O_4P_2$	342.39	1.004	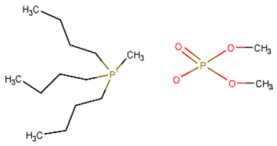
BMP	1-butyl-1-methylpyrrolidinium tris(pentafluoroethyl)trifluorophosphate	$C_{15}H_{20}F_{18}NP$	587.27	1.647	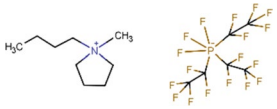
C12	Dodecanoic (Lauric) acid	$CH_3(CH_2)_{10}COOH$	200.32	1.007	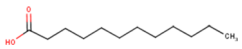

Table 2 pH, electrical conductivity, dynamic viscosity, density and OCP of the stainless steel sample in the formulated lubricants

Lubricant	Wt% of additive	pH	Conductivity (μS/cm)*	Viscosity (mPa.s)	Density (g/cm^3)	OCP before rubbing (V vs. Ag/AgCl)
WG	–	7.3	2.5	13.3	1.040	0.02
WG-AM	1	7.0	319.7	13.2	1.042	0.01
WG-PP	1	3.4	211.2	13.0	1.039	0.18
WG-BMP	1	7.0	109.3	13.3	1.045	0.00
WG-C12	0.1	4.7	4.3	13.3	1.041	0.03

*For comparison, the conductivity of tap water is ca 500 μS/cm and for seawater is ca 5000 μS/cm

is ≤ 1 ng/cm^2. The flow cell volume was about 40 μl. Stainless steel-coated AT-cut quartz crystals with a fundamental resonance frequency of 5 MHz from QSense (Biolin Scientific) were used. The experiments were performed at 0.05 ml/min flow rate maintained with a peristaltic pump. The resonance frequency and dissipation shifts were recorded with the time resolution of 2.7 s at the overtone numbers of 1, 3, 5 and 7 with the frequencies of 5, 15, 25 and 35 MHz, respectively. QCM-I sensors were cleaned by immersing in 1% Hellmanex III for 30 min, rinsing with distilled water, drying with Nitrogen gas and 10-min exposure to UV ozone cleaner. The QCM-I experiments were started by injecting the base lubricant for about 60 min to obtain a steady baseline and continued by injecting the formulated lubricant for about 20 min to measure the adsorption behaviour of the additives. The experiments were finished by switching to the base lubricant to remove the weakly adsorbed species and measure the mass of strongly adsorbed additive molecules. The QCM-I tests were conducted at least three times for each solution to check the repeatability of the results. For extracting the frequency drop related to changes in viscosity and density (from the base fluid to the formulated lubricant and vice versa), a calibration chart of density and viscosity of water/glycol mixtures with different water-to-glycol ratios has been prepared. Based on the viscosity and the density of each formulated lubricant, a water–glycol mixture with same viscosity–density product ($\mu \times \rho$) was chosen as baseline to avoid any frequency shift regarding bulk viscosity and density changes [23]. The in-situ QCM-I measurements enabled to measure not only the adsorbed mass on the surface but also the viscoelastic properties (viscosity and shear modulus) of the soft adsorbed layers [24]. MATLAB was used for developing a code to model the viscoelastic properties using a Voigt model for viscoelastic materials [24–26]. This model consists of a Newtonian damper and an elastic spring (following Hooke's law) connected in parallel and it represents a solid undergoing reversible, viscoelastic strain. Some assumptions to apply this model were made: Newtonian bulk solution, durable adsorption of the layer (no slip), evenly distribution of the adsorbed layer and homogeneous properties (viscosity and elasticity) of the adsorbed layer. In this model, initial values for the film parameters (density—ρ_A,

thickness—d_A, shear elastic modulus—μ_A, and shear viscosity—η_A), bulk liquid (ρ_B, μ_B) and quartz crystal (fundamental frequency—f_Q, ρ_Q, μ_Q) should be submitted as input and then the program calculates Δf^c (calculated frequency changes) and ΔD^c (calculated dissipation changes) for the selected overtones (minimum 3 overtones are needed for the calculation) following the model equations. The MATLAB fminsearch function finds the minimum of the error function (χ^2) between the calculated (Δf^c and ΔD^c) and the measured (Δf^m and ΔD^m) at each overtone by iterating on the initial values of the film parameters. More details of the implemented model are provided as supplemental information.

The tribological study was performed using a ball-on-flat reciprocating apparatus TriboCorr (Resmat Corporation, Canada) with a stroke length of 10 mm. The open circuit potential (OCP) before rubbing was measured during 1200 s versus an Ag/AgCl KCl saturated reference electrode. The sliding was established by rubbing an alumina ball of 6 mm diameter against the samples at a normal load of 20 N at room temperature with the frequency of 1 Hz during 5000 s, which is equal to 100 m sliding distance. The initial maximum contact pressure was 2.25 GPa and the calculated boundary lubricant film thickness using Hamrock–Dowson equation was less than the surface roughness of the stainless steel samples, indicating boundary lubrication regime [27]. At least two tests were performed for checking the repeatability of the results.

The volume loss of the samples was measured by means of an Alicona InfiniteFocus optical 3D microscope. The wear track volumes were measured using a reference line in 3 mm distance from both sides of the wear tracks. The average value of at least three measurements for each sample is reported as the average volume loss.

The wear tracks topography and cross-section were studied by a FEI Helios Nanolab DualBeam scanning electron microscope (SEM) and a focused ion beam (FIB). The carbon deposition, milling and polishing were carried out by using a gallium source and by means of SEM In Chamber Electronics (ICE) detector, secondary ions and secondary electrons were collected to produce the cross-section images. Moreover, FIB was used to prepare samples for S(T)EM examination. A scanning-transmission electron microscope; S(T)EM (Hitachi S-5500) was used to study the tribofilm formation at the maximum voltage of 30 kV.

The surface chemistry of different samples, inside and outside the wear tracks, was studied by X-ray Photoelectron Spectroscopy (XPS) using a Kratos Axis Ultra DLD. A monochromatic Al-Kα source with the current of 10 mA and voltage of 10 kV was used to perform the tests. The XPS sample chamber pressure was 1×10^{-9} Torr during the acquisitions [28]. Elemental survey acquisitions were performed with the pass energy of 160 eV with 2 sweeps and high-resolution regional acquisitions were carried out with pass energy of 20 eV, 7 sweep times and 0.1 eV step size for each element. Depth profile studies were performed using ion milling by Argon sputtering at the Argon pressure of 6.9×10^{-7} Torr and energy of 4 keV. CasaXPS software was used to analyse the XPS data and fit the curves. Full width at half maximum (FWHM) was kept constant for oxide phases of all elements, Shirley background subtraction was utilized for all quantifications and Gaussian/Lorentzian asymmetry was used for curve fittings [29].

3 Results

3.1 Adsorption Studies of the Additives on Stainless Steel

The quartz crystal microbalance (QCM) was first proposed by Gunter Sauerbrey to detect any mass changes (Δm) in the order of nanograms on the surface of quartz sensors [29]. This technique is able to quantify mass changes by measuring the shift in the resonance frequency of a quartz crystal. This change can be converted to mass by using Sauerbrey's equation:

$$\Delta f = -\left(\frac{2nf_0^2}{Z_q}\right)\times\Delta m \tag{1}$$

where f_0 is the fundamental frequency of the sensor, Z_q is the acoustic impedance of quartz (8.8×10^6 kg m^{-2} s^{-1}) and n is the overtone number [23]. It should be mentioned that Sauerbrey's equation is only valid when the adsorbed mass is completely rigid and does not show any viscoelastic behaviour. For studying adsorbed viscoelastic layers, non-gravimetric QCM should be utilized to extract the effect of the viscoelastic properties on the frequency changes and, by using the corrected values, the adsorbed mass or thickness can be calculated. Du and Johannsmann [30] have proposed a model by considering a thin viscoelastic film in a Newtonian liquid, and under certain simplifying assumptions proposed the following equation:

$$\Delta f = \frac{-2n}{Z_q}\times {f_0}^2\Delta m\,(1-\frac{Z_{liq}^2}{Z_f^2}) \tag{2}$$

where Z_{liq} and Z_f are the acoustic impedance of the adsorbed film and the bulk liquid, respectively. The equation is equivalent to the Sauerbrey equation with an additional term (in brackets) taking into account a viscoelastic correction [30]. Z_{liq} is dependent on the density and the viscosity of the bulk liquid and Z_f is dependent on the density of the adsorbed film and the shear modulus of the film. By plotting the ratio of bandwidth shift and frequency shift ($-\delta\Gamma/\delta f$) versus the overtone order n, the film's elastic compliance is obtained

from the slope. More details of the viscoelastic correction model are provided as supplemental information.

Recently, QCM measurements have been used by some researchers in lubrication science to investigate adsorbed layers either by Sauerbrey's equation or by using viscoelastic models [30–34]. The question to answer is: what plays the most important role in the frictional response, the thickness or the viscoelastic properties of the adsorbed layer?

Figure 1 illustrates the changes in frequency and dissipation during the injection cycle of Base lubricant/Base lubricant and additive/Base lubricant, in one set of tests for all the four additives used in this work. In the QCM tests, the water/glycol ratio of the base fluid has been calibrated to have the same viscosity–density product as the formulated lubricant. For the adsorbed mass quantification, the fundamental frequency gives better estimation and lower amount of underestimation, but the fundamental frequency data have not been used for viscoelastic modelling due to the higher effect of edge of sensors in this overtone. At higher overtones, the effect of edges decreases but the noise/data ratio increases.

By comparing the normalized frequencies plotted in Fig. 1 before and after rinsing the sensor with the base fluid, two different scenarios were found: (1) *initially adsorbed* mass and (2) *strongly adsorbed* mass. The *initially adsorbed* mass is represented by the frequency drop after injecting the solution of WG with additive and shows the amount of mass gained on the surface when the base lubricant contains an additive. This mass gain consists of both chemically and physically adsorbed species on the surface of the QCM sensor. The *strongly adsorbed* mass is represented by the frequency difference between the initial base line and the after-rinse frequency line, and illustrates the amount of strongly bonded molecules and ions in the absence of any further additive molecules in the system.

Table 3 shows, for each additive, the average and the standard deviation of the frequency drop after injection due to the *initial adsorption* (Δf_i), the frequency drop after rinsing (Δf_s), the mass changes related to these frequency drops (i.e. *initially adsorbed mass* (Δm_i) and *strongly adsorbed mass* (Δm_s)), the number of adsorbed molecules (Δn_i and Δn_s) calculated from the adsorbed mass values by considering the molecular weight of the additives, and also the proportion of the *strongly adsorbed* molecules to all initial-adsorbed molecules ($\Delta n_s/\Delta n_i$). The mass changes are calculated using the viscoelastic corrected equation (Eq. 2).

AM showed the lowest *initially adsorbed* mass and no *strongly adsorbed* mass was observed after rinsing. PP showed the highest *initially adsorbed* mass and about 21% of it remained on the surface after rinsing with the base fluid. BMP had only a slightly higher *initially adsorbed* mass compared to AM, but about 27% of the mass was *strongly adsorbed* and remained after rinsing. Even though C12 showed similar *initially adsorbed* mass to AM and BMP, due to its lowest molecular weight, the number of *initially adsorbed* molecules was high. Furthermore, about 45% of these adsorbed molecules had a strong bonding to the surface of stainless steel and remained after rinsing.

The variations in dissipation during the QCM-I tests are also presented in Fig. 1. The dissipation number can be a qualitative indicator of the rigid or viscoelastic behaviour of the adsorbed layers. The dissipation number (ΔD) was $(4.0 \pm 0.1) \times 10^{-6}$ for AM, $(4.7 \pm 1.1) \times 10^{-6}$ for BMP, $(7.4 \pm 0.4) \times 10^{-6}$ for PP and $(2.4 \pm 0.4) \times 10^{-6}$ for C12.

3.2 Friction and Wear

The frictional and wear behaviour of austenitic stainless steel 316L under the harsh boundary conditions in the presence of the base lubricant (distilled water and glycol) and the formulated lubricants (base and ILs or OFG) are presented in Fig. 2.

It can be observed that the base lubricant without any additives showed the poorest frictional behaviour but the lowest wear. The coefficient of friction of the base lubricant was stable at about 0.30 and by adding 1 wt% of AM and PP, it reduced to 0.22 (27%) and 0.23 (23%), respectively. The friction behaviour of the BMP-containing lubricant (WG-BMP) consists of two different regions: In the first 2000 cycles friction was stabilized at about 0.18 (ca. 40% lower than the base fluid) and between 2000 and 2800 cycles, a continuous reduction in friction is observed reaching a value of 0.11 (63% reduction) in the last 2000 cycles of rubbing. For the lubricant containing dodecanoic acid (WG-C12), the coefficient of friction fluctuated between 0.12 and 0.18 during the first 2000 cycles finally stabilizing at about 0.12. As for wear, the base lubricant showed the lowest wear rate of 1.1×10^{-5} mm^3/Nm and by adding PP, AM, BMP and C12 it increases to 4.8×10^{-5}, 4.1×10^{-5}, 1.2×10^{-5} and 2.1×10^{-5} mm^3/Nm, respectively.

3.3 Wear Topography

Figure 3 shows the SEM images of the worn area of 316L steel tested in the base lubricant and the formulated lubricants. The wear track topography of the base lubricant shows adhesive wear as the dominant mechanism, but some marks of abrasive grooves are also observable. The wear mechanism is completely different for WG-AM and WG-PP: severe ploughing, smearing, plastic deformation and abrasive grooves are the main features in the wear tracks which might be due to the oxidation of the wear debris. In the case of the tests with WG-BMP, a very smooth surface on the wear track is observed. The wear track of the sample tested in WG-C12 is not as smooth as WG-BMP, but obviously

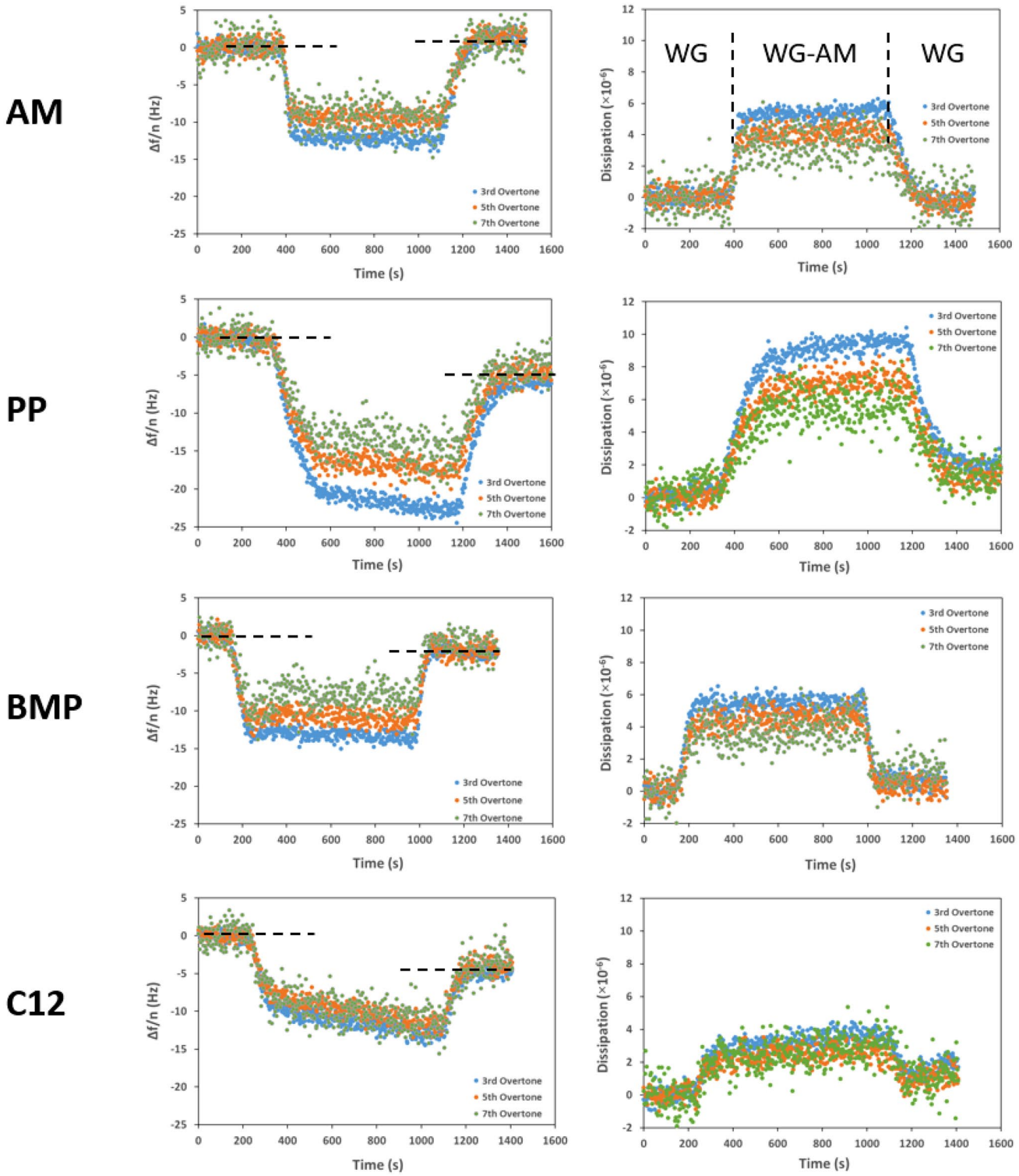

Fig. 1 Evolution in normalized frequency (left side) and dissipation (right side) during QCM analysis of WG and additive solutions. The 3rd, 5th and 7th overtones are illustrated. Only one set of results are shown for clarity, all three repetitions were very similar

less signs of ploughing and folds are observed representing less plastic deformation during sliding, than in WG-AM and WG-PP.

A more detailed characterization of the friction transition period of the sample tested with WG-BMP was done. A new test was performed for only 1400 cycles (before the

Table 3 Initial- and strongly adsorbed mass and number of the adsorbed molecules extracted from the QCM-I measurements

Additive	Δf_i (Hz)	Δf_s (Hz)	Δm_i (ng/cm^2)	Δm_s (ng/cm^2)	Δn_i (molecules/cm^2)	Δn_s (molecules/cm^2)	$\Delta n_s/\Delta n_i$ (%)
AM	10.0 ± 0.5	–	185.4 ± 9.1	–	$(4.87 \pm 0.24) \times 10^{14}$	–	
PP	18.7 ± 0.5	4.0 ± 0.7	394.4 ± 11.5	84.5 ± 15.0	$(6.95 \pm 0.20) \times 10^{14}$	$(1.49 \pm 0.20) \times 10^{14}$	21 ± 4
BMP	12.2 ± 2.5	3.4 ± 0.5	231.6 ± 46.9	64.3 ± 9.9	$(2.38 \pm 0.48) \times 10^{14}$	$(0.65 \pm 0.10) \times 10^{14}$	27 ± 2
C12	11.0 ± 1.4	4.9 ± 0.5	194.4 ± 24.1	88.1 ± 9.7	$(5.91 \pm 0.73) \times 10^{14}$	$(2.65 \pm 0.30) \times 10^{14}$	45 ± 3

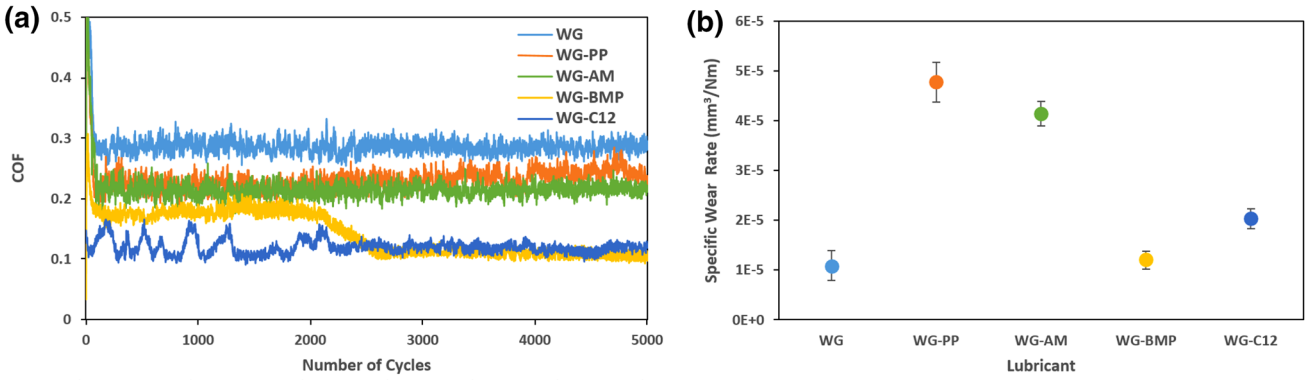

Fig. 2 Coefficient of friction evolution with time (**a**) and specific wear rate (**b**) of 316L stainless steel in different lubricants

drop in friction is observed (see Fig. 2a)). The top view and FIB cross-sectional images of the wear track of WG-BMP-5000 cycles and WG-BMP-1400 cycles are shown in Fig. 4. As reference, the sample tested with WG-PP-5000 cycles is shown in Fig. 4 as well. The top view images show clear wear marks, abrasive grooves, severe surface damage and cracks in WG-PP and milder abrasive signs and surface cracks in WG-BMP after 1400 cycles. This abrasive damage might be generated by oxidized wear debris in the case of PP compared to BMP. This is in agreement with the higher conductivity of WG-PP solution and lower pH of the PP-containing lubricant. The top view of the sample tested in WG-BMP for 5000 cycles shows very smooth surface without any surface damage.

The FIB cross-section micrographs reveal cracks and surface/sub-surface damages in the wear track of WG-PP. Moreover, the high initial Hertzian contact pressure of 2.25 GPa together with the higher shear stress in the case of WG-PP (due to the higher coefficient of friction) resulted in higher degree of recrystallization. On the other hand, the FIB cross-section of WG-BMP after 1400 cycles shows less surface roughness, limited crack propagation and sub-surface damages and lower degree of dynamic recrystallization. The cross-section of WG-BMP after 5000 cycles shows a remarkably smooth surface, very slight recrystallization and no sign of surface cracks and sub-surface damages. It seems that the highly recrystallized regions in the top 1 µm of WG-BMP sample after 1400 cycles have been removed during the wear cycles of the transition period, and friction was drastically reduced. The reduction in coefficient of friction resulted in a decrease in shear stress and consequently a larger grain size in the sub-surface region was observed.

The smooth surface observed on the BMP tested sample during 5000 cycles and the very low wear rate might indicate some kind of tribofilm formation. In order to investigate it, this sample was examined by S(T)EM (Fig. 5). As the acceleration voltage in S(T)EM is lower than that for TEM, 30 kV compared to 200 kV, thinner lamella samples should be prepared to let the electrons go through the sample and reach the TEM detector of the S(T)EM instrument. A tribofilm of around 20 nm has been found in the wear track of the stainless steel tested with WG-BMP, as observed in Fig. 5, which can be the responsible for the decrease in friction and wear. Interestingly, the sample tested with C12 also shows a rather smooth surface, low friction and low wear rate. This sample has not been investigated by S(T)EM, but in a previous work, a tribofilm was found on the surface of stainless steel 316L tested with a water–glycol formulated with palmitic acid (C16) [35]. However, the concentration of C16 was higher (1 wt%) than in the present work and the tribofilm formed with C12 can be expected to be thinner.

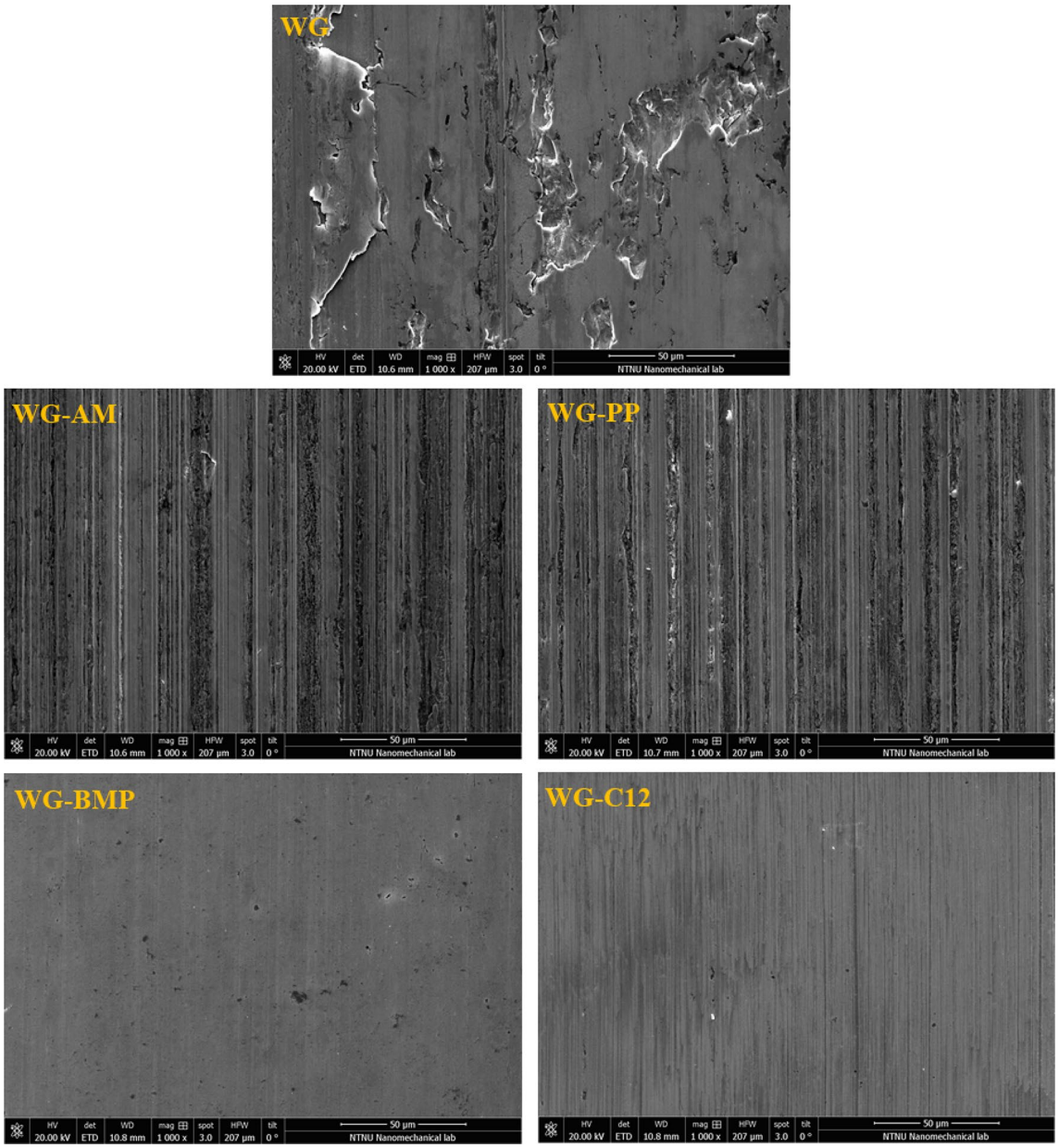

Fig. 3 Wear track morphology of 316L stainless steel specimens tested with reciprocal pin-on-plate tribocorr machine with the base lubricant and lubricants formulated by the ILs and C12

4 Discussion

4.1 Effect of Surface Chemical Composition on Wear

Understanding the surface chemical composition of the metal in each lubricant can be the key to explain frictional behaviour of different additives. Stainless steels form a passive film on their surfaces and it is well known that this is the main reason for the good corrosion resistance of these alloys [36]. The composition of passive layers on stainless steels vary depending on the media they are in contact with and the alloying elements, but typically they consist of chromium oxide, other metal oxides and chromium hydroxide. The hydroxides in passive films can act as weak points in the wear track, accelerating corrosion and tribocorrosion degradation mechanisms and facilitating more volume loss [37, 38].

Figure 6 shows the Pourbaix diagram of chromium at 25 °C indicating the expected stable phase in equilibrium on the surface of 316L stainless steel in the presence of the different lubricants investigated in this study. Based on the pH of the solutions and the open circuit potential (OCP)

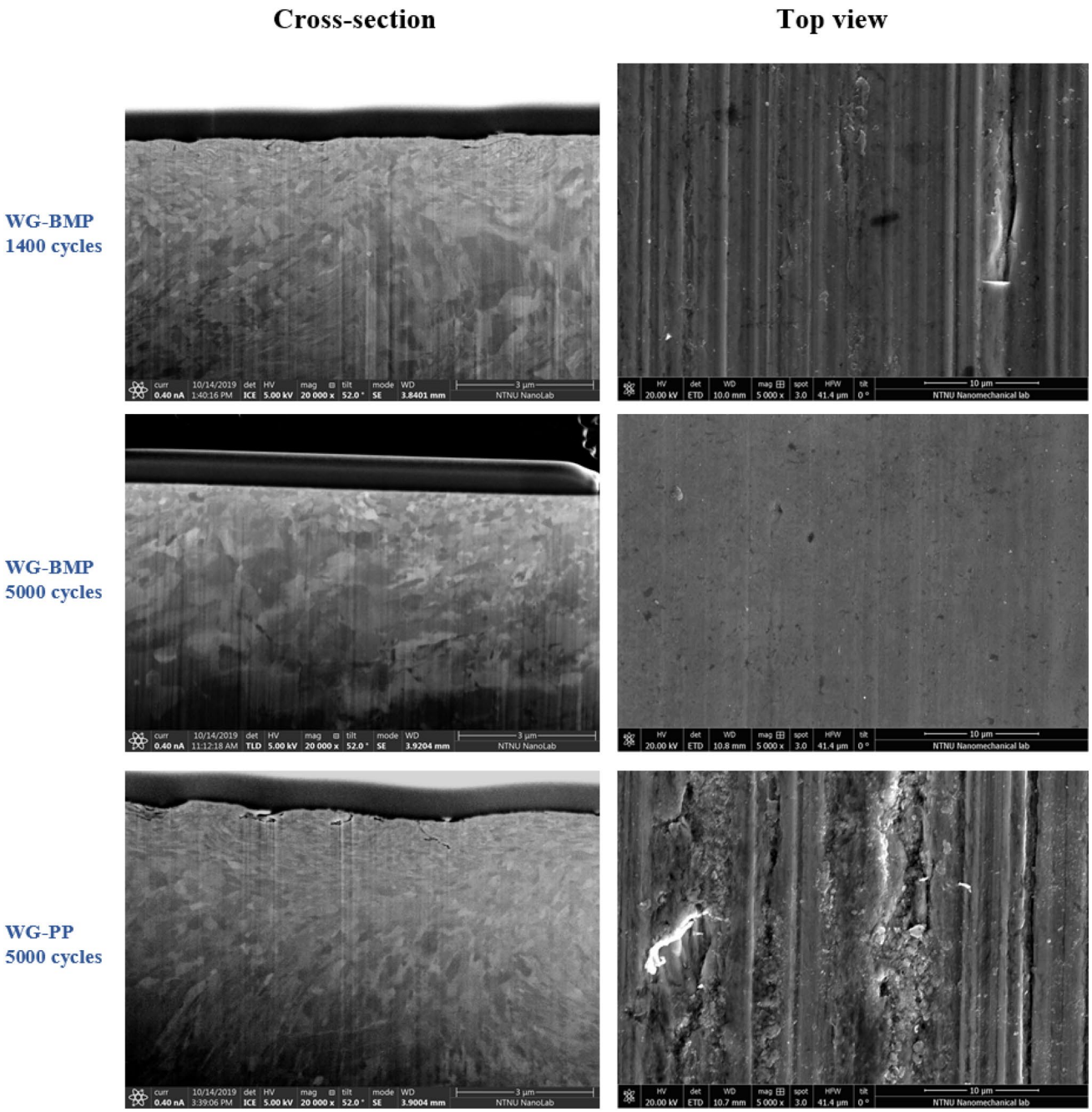

Fig. 4 FIB cross-section and top view of the wear track of WG-BMP-1400 cycles, WG-BMP-5000 cycles and WG-PP-5000 cycles

of the 316L in the lubricants (Table 2), the expected stable chromium compound in the passive film can be extracted from the Pourbaix diagram.

Figure 6 shows that WG, WG-AM and WG-BMP are expected to create a chromium oxide (Cr_2O_3) stable phase on the surface of stainless steel. For WG-PP, chromium hydroxide ($Cr(OH)_3$) would be the dominant phase on the surface and for WG-C12, the system is in the border of chromium oxide and chromium hydroxide. The stainless steel used in this work contains 2–3 wt% of molybdenum (Mo). Mo stabilizes chromium oxides in the passive film by decreasing the formation of chromium hydroxide and forming a molybdenum oxide [36, 38]. It has already been suggested by Zavieh and Espallargas, when testing stainless steel 316L in seawater under different mechanical conditions, that higher relative concentration of $Cr(OH)_3$ in the passive film results in a thicker and more brittle

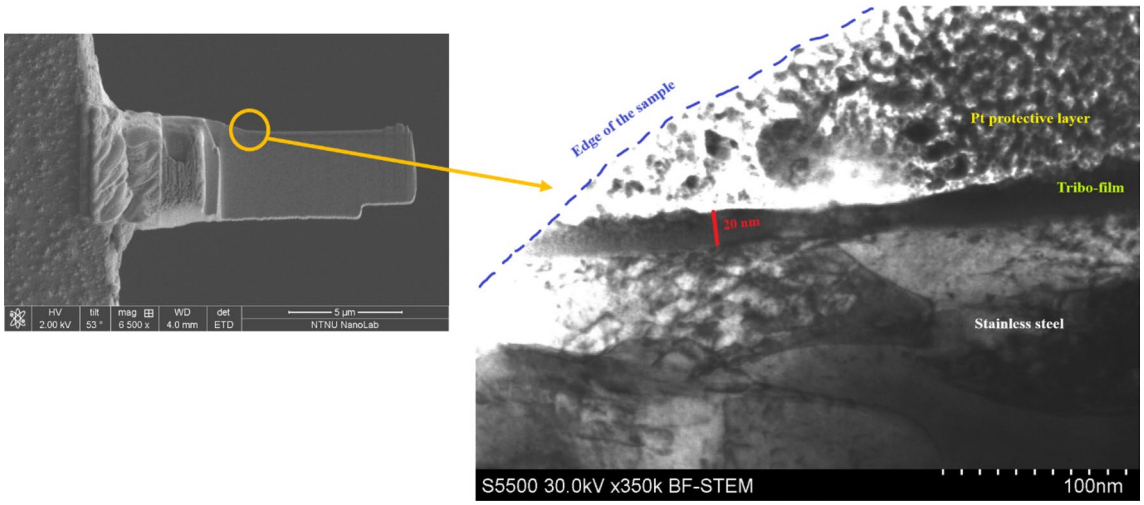

Fig. 5 FIB prepared lamella and S(T)EM transmission electron image from the tribofilm of WG-BMP-5000 cycles sample

passive film [37]. This thicker and more brittle passive film hinders the surface plasticity resulting in more wear.

Therefore, X-ray photoelectron spectroscopy (XPS) outside the wear tracks has been performed in this work to investigate the composition of the passive films in the presence of different additives (PP as it is located in the chromium hydroxide region and BMP as it is located in the chromium oxide region). Figure 7 shows the high-resolution XPS spectra of Cr and Mo outside the wear track of the samples tested in WG-PP and WG-BMP. The Cr spectra have been plotted in the binding energy range of 575–781 eV, which is relevant for peak positions of chromium oxide and hydroxide phases. The XPS spectra show the chemical composition of the passive films and it is in good agreement with the data extracted from the Pourbaix diagram. The Cr spectra show the presence of Cr_2O_3, CrO_3 and $Cr(OH)_3$ phases on the surface of both samples. The presence of CrO_3 cannot be predicted based on the Pourbaix diagram, but it has been found that CrO_3 can co-exist with Cr_2O_3 in the glassy passive layers because of their similar standard enthalpies [37, 38].

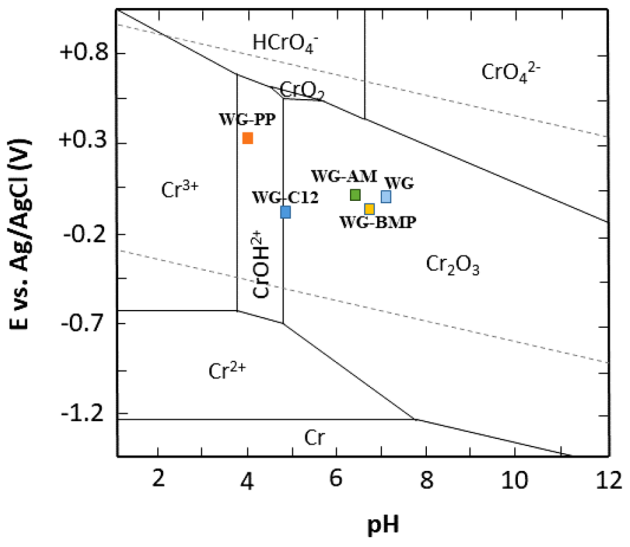

Fig. 6 Pourbaix diagram of chromium at 25 °C, the studied lubricants are located in the diagram based on their OCP and pH value reported in Table 2

Figure 7 clearly shows that in the presence of PP, the main phase in the passive film is $Cr(OH)_3$ and in the presence of BMP, Cr_2O_3 is the dominant phase. The high-resolution Mo spectra reveal the presence of Mo in the passive film of WG-BMP, but no sign of Mo peaks was found in the case of WG-PP. The presence of Mo in the passive film and the enhanced oxidation of Mo in WG-BMP compared to WG-PP contributes to less oxidation of the wear debris, leading to less wear-accelerated corrosion and milder wear topography in WG-BMP compared to WG-PP (top views in Fig. 4).

As it was mentioned in Sect. 3.2 (Fig. 2b), the base lubricant (WG) showed the lowest wear and a drastic increase in wear was observed for PP and AM, whereas the increase in wear for BMP was the lowest and it was intermediate for C12. These effects are in good agreement with the passive film composition, the pH and the conductivity of the different lubricants (Table 2), where an increase of two orders of magnitude in the electrical conductivity of the solution by adding the ILs to the base lubricant is observed. The base lubricant had a pH of 7.3 and adding AM and BMP did not affect the pH of the base lubricant. However, PP and C12 resulted in a drastic decrease in pH to 3.4 and 4.7, respectively. The acidic behaviour and the high electrical conductivity of WG-PP can be a reason for higher volume loss in this lubricant. Since the anionic moieties of AM and PP are

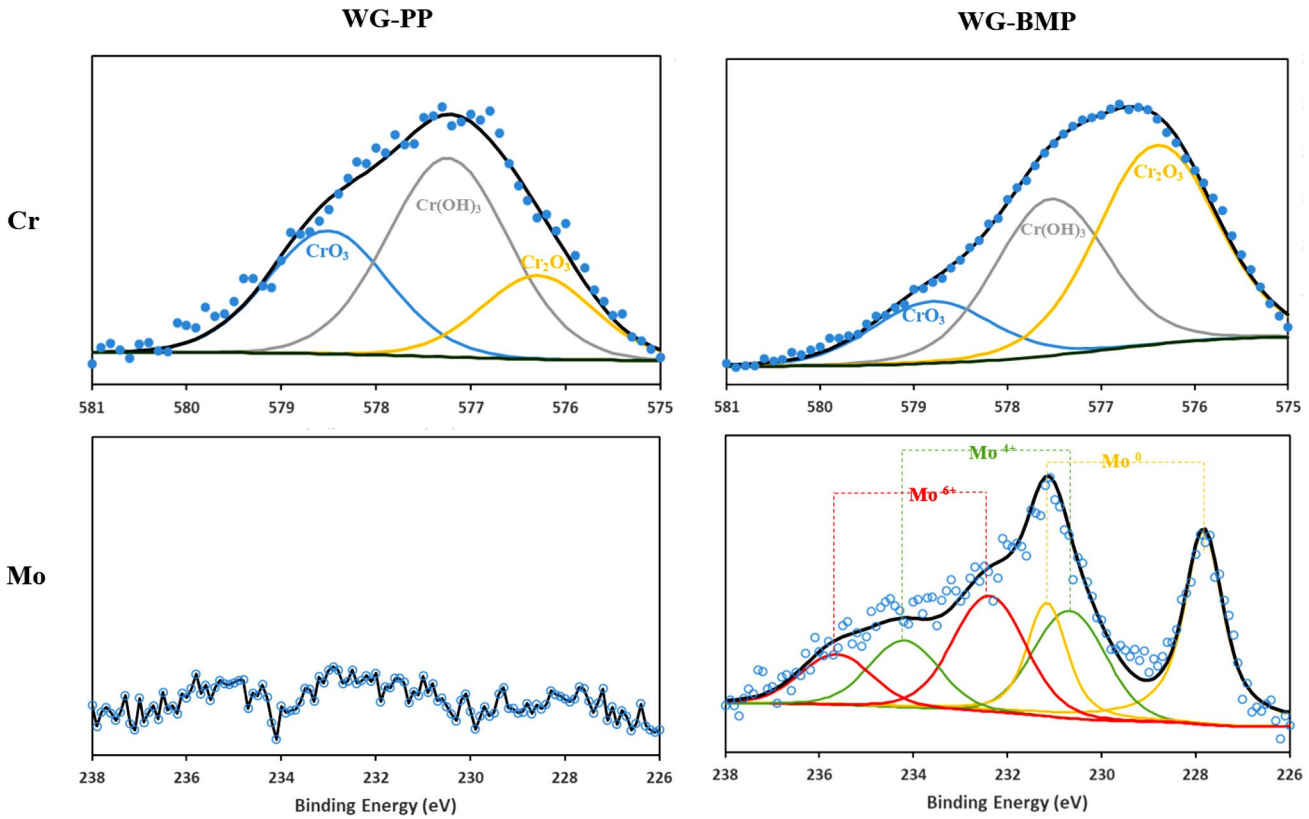

Fig. 7 High-resolution XPS spectra of Cr and Mo outside the wear track of the samples tested in WG-PP and WG-BMP

similar, the ionic interactions between the phosphonium-base cation of PP and the water molecules could result in the formation of phosphoric acid dropping the pH of the solution. The acidification of the solution together with the high electrical conductivity might enhance the oxidation of the wear debris particles, leading to abrasion of the surfaces and increasing wear rates. The pH of WG-C12 was also acidic, but the very low electrical conductivity of this lubricant might restrict the interaction of the carboxylic acid with the surface of the stainless steel hindering the oxidation of the wear debris. On the other hand, AM despite having the same pH as the base lubricant, the electrical conductivity was the highest of all ILs and this resulted in a very high wear rate, similar to WG-PP.

However, the wear rate of WG-BMP is relatively similar to the base lubricant (1.2×10^{-5} mm^3/Nm), whereas the electrical conductivity is ca. 2 order of magnitude higher than the base lubricant. Among all ILs, BMP showed the lowest electrical conductivity and the highest content of chromium oxide in the passive film. This low wear rate can be related to the change in the frictional response after 2000 cycles of sliding as the result of the tribofilm formation (Fig. 5). In the case of C12, similar values of wear and friction as in the BMP case are found despite their different chemical composition in the passive film. Therefore, other effects than just passive film composition, pH and conductivity of the lubricants are to be expected to play a role in the friction and wear performance.

4.2 The Friction and Wear Mechanism: Adsorbed Layer Versus Tribofilm Formation

Functionality of ionic liquids as lubricating additives depends on their ability to form either an adsorbed layer or a protective tribofilm on the surface of the wear track [15]. The frictional reducing behaviour of adsorbed layers depends not only on the thickness of the layer, but also on the rigidity and durability of the layer in loading conditions. Parameters such as surface chemistry and surface charge of mating surfaces, polarity of base lubricant, polarity of anionic and the cationic parts of the IL could define surface coverage, thickness and viscoelastic behaviour of adsorbed layers between two mating surfaces.

Ionic liquids, due to their ionic nature and high dipole moment, are known to have high tendency to be adsorbed on the surface of metals [15]. Thus, the brushy-like soft adsorbed layers formed by the orientation of the anionic and cationic moieties of the ILs have been considered as an important friction-modifying mechanism for these substances [16]. It should be noted that the thickness of the

adsorbed layers is in the order of a single-layer or multi-layers of ions and therefore a surface characterization technique with the resolution of less than 10 nm is needed to study the adsorption behaviour. In this work, QCM has been the chosen technique.

Comparing the frequency evolution patterns shown in Fig. 1, it is clear that water was able to dissociate the additive's structure to free ionic species for PP and C12. This is illustrated by the two-step behaviour of the adsorption kinetics since the additive species continue to occupy the surface sites even after passing the first step of fast adsorption. On the other hand, for AM and BMP, the adsorption was limited to the first step and after passing this threshold, no more interaction was observed on the surface. Moreover, *strongly adsorption* happened in PP, BMP and C12. This behaviour in C12 and PP can be attributed to the dissociation of the additive's structure resulting in species with higher polar moment. However, the higher tendency of BMP to be adsorbed on the surface of stainless steel could be due to the fluorine atoms in the anionic part of BMP. The high electronegativity of fluorine can lead to stronger adsorption on the positively charged surface of the metal-coated QCM sensor.

The formation of a completely rigid film on the surface of QCM sensors results in a frequency drop without any change in bandwidth (which is equal to no change in dissipation). In the case of adsorbed layers, usually dissipation changes (ΔD) smaller than 2×10^{-6} are considered as a rigid film [23, 33]. Therefore, viscoelastic brushy layers can be expected for dissipation changes higher than 2×10^{-6}. As it can be seen in Fig. 1, the dissipation changes (ΔD) for all studied IL containing lubricants were higher than 2×10^{-6} indicating that a viscoelastic layer was formed on the surface. The average dissipation changes for the different additives were 4.0×10^{-6}, 7.4×10^{-6}, 4.7×10^{-6} and 2.4×10^{-6} for AM, PP, BMP and C12, respectively. Interestingly, the ΔD value for C12 was the smallest of all additives indicating a more rigid behaviour of the adsorbed layer. The results of the viscoelastic modelling for one set of tests are shown in Fig. 8. The thickness, viscosity and elastic modulus numbers derived from the two tests performed for each additive are presented in Table 4.

PP shows the highest thickness and BMP and C12-formed adsorbed layers with the lowest thickness. On the other hand, C12 forms the most viscous layer. The elastic modulus of the adsorbed layers is the most critical parameter that reveals the viscoelastic behaviour of brushy soft layers. C12-adsorbed layer shows an average elastic modulus of about 2143 kPa, which is at least three times higher than the values for the ILs. Therefore, C12 forms a more rigid layer compared to PP, AM and BMP. Higher rigidity and elastic modulus of C12-adsorbed layer can be the reason for lower coefficient of friction of C12 compared to ILs (Fig. 2a). Therefore,

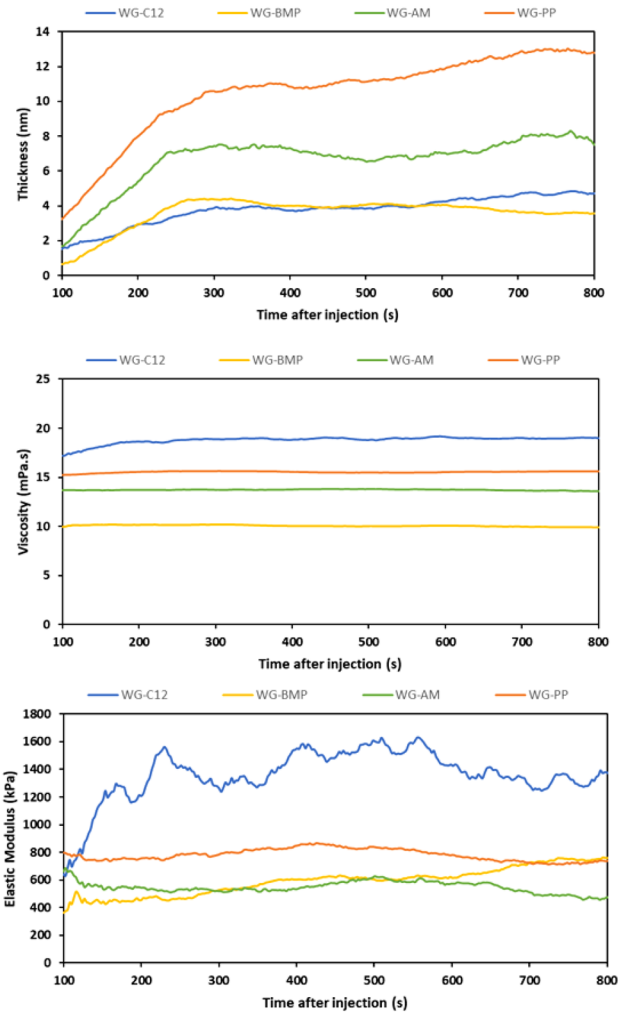

Fig. 8 Thickness, viscosity and elastic modulus of the adsorbed additive layers derived from the viscoelastic modelling

Table 4 Viscoelastic properties derived from the applied model on the QCM-I data

Additive	thickness (nm)	Viscosity (mPa.s)	Elastic modulus (kPa)
AM	7.0 ± 0.3	13.7 ± 0.1	566 ± 30
PP	12.3 ± 0.7	15.6 ± 0.1	674 ± 79
BMP	6.2 ± 1.8	10.0 ± 0.1	389 ± 181
C12	3.3 ± 1.0	21.5 ± 2.3	2143 ± 513

by comparing the surface adsorption data and the frictional behaviour of the additives, it can be concluded that the thickness of the adsorbed layer is not the most important parameter in frictional functionality of additives if the *adsorbed layer* mechanism is the main responsible for the frictional response of the system. However, the thickness of the *strongly adsorbed layer* and the viscoelastic properties of the adsorbed layer are the most important parameters to

be considered. C12 showed the best friction-modifying ability: even though its initial adsorption mass was the lowest, however, about 45% of the *initially adsorbed* species were strongly bonded and remained adsorbed to the stainless steel surface after rinsing.

Among the three ILs studied in this work, BMP showed the best frictional response close to C12. In addition, this is the only IL forming a tribofilm on the stainless steel surface (Fig. 7). The QCM adsorption study of BMP shows on the other hand the lowest values of viscosity and elastic modulus, and similar number of *strongly adsorbed* molecules as PP on the surface after rinsing. This might indicate that the adsorption kinetics have played a role in this case. It should be noted that all QCM adsorption studies have been conducted in a static state. In the tribological tests (dynamic), the adsorbed species are continuously removed from the contact and in order to have an effect on the frictional response, they need to replenish the contacting surfaces. Thus, the kinetics of re-adsorption plays a crucial role on the friction-modifying ability of the additives. To model the adsorption kinetics, a first-order rate equation reduced from Langmuir kinetics was used [39, 40]:

$$\frac{d\theta_t}{dt} \approx k_1\left(\theta_e - \theta_t\right) \tag{3}$$

in which θ_e and θ_t are the occupied adsorption sites at equilibrium and time t, and k_1 is the first-order adsorption kinetic constant. By integration of Eq. (3), a logarithmic dependency of the amount of mass adsorbed on the surface to time is obtained by means of a kinetic constant:

$$ln\left(q_e - q_t\right) = ln\left(q_e\right) - k_1 \tag{4}$$

where q_t and q_e are the mass adsorbed at time t and in equilibrium. In Fig. 9, $\ln(q_e - q_t)$ has been plotted during the first 120 s for one set of the adsorption tests. The adsorption kinetic constants were calculated by fitting Eq. (4) to the data acquired by QCM. The fitting resulted in k_1 factors of $0.0095 \pm 0.0013\ s^{-1}$ for PP, $0.0316 \pm 0.0016\ s^{-1}$ for BMP and $0.0137 \pm 0.0019\ s^{-1}$ for C12. Even though the adsorbed layer of BMP shows lower viscosity and rigidity than C12 and the lowest of all ILs, this IL reaches similar values of friction and lower wear than C12. The higher adsorption kinetics of BMP can be the reason for better frictional response of BMP compared to the two other ILs and in addition, it can be the reason for the tribofilm formation.

As it has been shown above, and as already stated in literature, ILs can either adsorb on the surface of metals or form a tribofilm. In this work, it has been demonstrated that the adsorption kinetics are the critical parameter to determine whether an IL additive will lead to only an adsorbed layer on the surface or if it will lead to a tribofilm formation. If only an adsorbed layer is formed on the surface, this needs to be

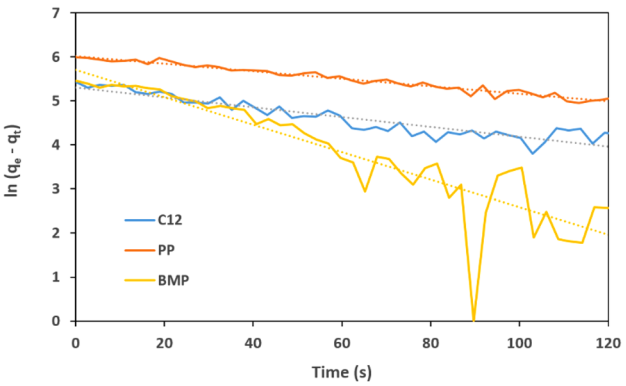

Fig. 9 Adsorption kinetics of three additives on the surface of stainless steel-coated QCM sensor

both rigid and viscous enough to provide with low friction and low wear. However, the tribofilm formation process consists of several steps such as adsorption of the additives on the surface, break-down of the additive's chemical structure due to high temperature or pressure in the contact, reaction of the new product from the break-down of the additive and some surface species and formation of a new structure on the surface. Therefore, fast kinetics of the adsorption process facilitates the stability of the adsorbed additive species in the contact area during sliding. As Fig. 9 shows, BMP has the fastest adsorption kinetics, and this can be one reason for tribofilm-forming ability for this IL.

5 Conclusions

Three different ionic liquids as additives in a water-based lubricant have been tested and compared with a well-known organic friction modifier. The goal of this work was to investigate the friction and wear mechanisms of ionic liquids since in literature two possible routes are proposed, i.e. physisorption or tribofilm formation. The frictional behaviour and wear behaviour have been studied in boundary lubricating conditions. The surface adsorption of the additives has been studied by means of QCM-I technique and the surface and sub-surface of the worn metal samples were investigated by SEM, FIB, S(T)EM and XPS. The ionic liquids studied in this work led to both friction and wear mechanisms, adsorbed layers and tribofilm formation. The reasons behind this behaviour are different for each ionic liquid and are summarized in the following conclusions:

- The organic friction modifier (C12) showed the best frictional and wear performance of all additives tested. It created the most rigid adsorbed layer of all additives on the surface of the stainless steel-coated QCM sensor. This and the high amount of strongly adsorbed

mass after rinsing (45%) are the main reasons for its good frictional and wear performance.

- For the ionic liquids, two different surface adsorption behaviour on stainless steel-coated QCM sensors were observed: (1) no *strongly adsorbed* mass in the case of AM and (2) *strongly adsorbed* mass in the case of PP (21%) and BMP (27%) after rinsing. This shows that AM did not dissociate in the lubricant media hindering the adsorption of this ionic liquid to the metal surface, whereas PP did dissociate allowing the free polar moieties to adsorb on the metal surface. It is unknown whether BMP dissociated in the water media, however, the high electronegativity of the anionic part of BMP due to the presence of fluorine atoms might also have facilitated the adsorption of this ionic liquid to the metal.
- In the case of PP, despite its high amount of adsorbed mass on the metal surface, the low pH and the high conductivity of the lubricant resulted in poor frictional and wear behaviour. The Pourbaix diagram for Cr in the pH and electrode potential conditions for this media showed chromium hydroxide as the most stable phase for the passive film composition on the stainless steel (confirmed also by XPS). This hindered the presence of Mo on the surface of the metal and resulted in a more brittle passive film leading to more wear.
- Among all the ionic liquids, the best performing one was BMP, which resulted in similar values of friction and wear as C12 after a transition period at 2000 sliding cycles. The better frictional behaviour of BMP has been found to be related to its faster adsorption kinetics. This allowed a fast replenishment of the contact with the additive, facilitating the formation of a thick tribofilm on the stainless steel surface.
- Among all ionic liquids investigated in the present work as additives in a water-based lubricant, the mechanism resulting in the best frictional and wear performance was the tribofilm formation.

Acknowledgements The authors would like to acknowledge the financial support from the M-ERA.NET GreenCOAT project with Project Number 4153 as well as the financial support from The Research Council of Norway. Norwegian Micro- and Nano-fabrication facility, NorFab, is also acknowledged for providing the characterization facilities.

Funding The project is funded by The Research Council of Norway in the form of M-ERA.NET GreenCOAT project with Project Number 4153.

Compliance with Ethical Standards

Conflict of interest The authors declare that they have no known competing financial interests that could have influence on the work reported in this paper.

References

1. Singh, H., Gulati, I.L.: Tribological behavior of base oils and their separated fractions. Wear (1991). https://doi.org/10.1016/0043-1648(91)90130-M
2. Zhou, Y., Dyck, J., Graham, T.W., Luo, H., Leonard, D.N., Qu, J.: Ionic liquids composed of phosphonium cations and organophosphate, carboxylate, and sulfonate anions as lubricant antiwear additives. Langmuir (2014). https://doi.org/10.1021/la5032366
3. Rudnick, L.R.: Lubricant additives: Chemistry and Applications, 2nd edn. Taylor & Francis, London (2009)
4. Zabawski, E.: Seren-ZDDP: life is full of accidental discoveries. Tribol. Lubr. Technol. **73**, 6 (2017)
5. Spikes, H.: The history and mechanisms of ZDDP. Tribol. Lett. **17**, 469 (2004)
6. Zhou, Y., Qu, J.: Ionic liquids as lubricant additives: a review. ACS Appl. Mater. Interfaces (2017). https://doi.org/10.1021/acsami.6b12489
7. Dorr, N., Merstallinger, A., Holzbauer, R., Pejakovic, V., Brenner, J., Pisarova, L., Stelzl, J., Frauscher, M.: Five-stage selection procedure of ionic liquids for lubrication of steel-steel contacts in space mechanisms. Tribol. Lett. (2019). https://doi.org/10.1007/s11249-019-1185-4
8. Wasserscheid, P., Welton, T. (eds.): Ionic Liquids in Synthesis, 2nd edn. Wiley, Weinheim (2008)
9. Ye, C., Liu, W., Chen, Y., Yu, L.: Room-temperature ionic liquids a novel versatile lubricant. Chem. Commun. (2001). https://doi.org/10.1039/b106935g
10. Somers, A., Howlett, P., MacFarlane, D., Forsyth, M.: A review of ionic liquid lubricants. Lubricants (2013). https://doi.org/10.3390/lubricants1010001
11. Bermudez, M.D., Jimenez, A.E., Sanes, J., Carrion, F.J.: Ionic liquids as advanced lubricant fluids. Molecules (2009). https://doi.org/10.3390/molecules14082888
12. Qu, J., Luo, H., Toops, J.T., West, B.H., Blau, P.J., Dai, S., Papke, B.L., Gao, H., Kheireddin, B., Chen, C.: Ionic liquids as multifunctional lubricant additives to enhance engine efficiency. Final Rep NFE-12-03876 (2016). https://doi.org/10.2172/1246776
13. Xiao, H.: Ionic liquids lubricants: basics and applications. Tribol. Trans. (2017). https://doi.org/10.1080/10402004.2016.1142629
14. Perkin, S., Albrecht, T., Klein, J.: Layering and shear properties of an ionic liquid, 1-ethyl-3-methylimidazolium ethylsulfate, confined to nano-films between mica surfaces. Phys. Chem. Chem. Phys. (2010). https://doi.org/10.1039/b920571c
15. Huang, G., Yu, Q., Ma, Z., Cai, M., Liu, W.: Probing the lubricating mechanism of oil-soluble ionic liquids additives. Tribol. Int. (2017). https://doi.org/10.1016/j.triboint.2016.08.027
16. Liu, X., Zhou, F., Liang, Y., Liu, W.: Tribological performance of phosphonium based ionic liquids for an aluminum-on-steel system and opinions on lubrication mechanism. Wear (2006). https://doi.org/10.1016/j.wear.2006-03.018
17. Perkin, S.: Ionic liquids in confined geometries. Phys. Chem. Chem. Phys. (2012). https://doi.org/10.1039/C2CP23814D
18. Mu, Z., Zhou, F., Zhang, S., Liang, Y., Liu, W.: Effect of the functional groups in ionic liquid molecules on the friction and wear behavior of aluminum alloy in lubricated aluminum-on-steel contact. Tribol. Int. (2005). https://doi.org/10.1016/j.triboint.2004.10.003
19. Jiang, D., Hu, L., Feng, D.: Crown-type ionic liquids as lubricants for steel-on-steel system. Tribol. Lett. (2011). https://doi.org/10.1007/s11249-010-9726-x
20. Qu, J., Chi, M., Meyer, H.M., Blau, P.J., Dai, S., Luo, H.: Nanostructure and composition of tribo-boundary films formed in ionic liquid lubrication. Tribol. Lett. (2011). https://doi.org/10.1007/s11249-011-9800-z

21. Lawes, S.D.A., Hainsworth, S.V., Blake, P., Ryder, K.S., Abbott, A.P.: Lubrication of steel/steel contacts by choline chloride Ionic liquids. Tribol. Lett. (2010). https://doi.org/10.1007/s11249-009-9495-6
22. Bernat, S., Armada, S., Espallargas, N.: Effect of contamination on the friction and wear of carboxylic acids in aqueous lubricants. Tribol. Lett. (2018). https://doi.org/10.1007/s11249-018-1116-9
23. Technical Note: The principles of QCM-I, Quartz crystal microbalance with impedance analysis. https://www.gamry.com/assets/Uploads/QCM-I-principles.pdf.
24. Saftics, A., Prosz, G.A., Turk, B., Peter, B., Kurunczi, S., Horvath, R.: In-situ viscoelastic properties and chain conformation of heavily hydrated carboxymethyl dextran layers: a comparative study using OWLS and QCM-I chips coated with waveguide material. Sci. Rep. (2018). https://doi.org/10.1038/s41598-018-30201-6
25. Voinova, M.V., Rodahl, M., Johnson, M., Kasemo, B.: Viscoelastic acoustic response of layered polymer films as fluid-solid interfaces: continuum mechanics approach. Phys. Scr. (1999). https://doi.org/10.1238/Physica.Regular.059a00391
26. McNamara, T.P., Blanford, C.F.: A sensitivity metric and software to guide the analysis of soft films measured by a quartz crystal microbalance. Analyst. (2016). https://doi.org/10.1039/C6AN00143B
27. Hamrock, B.J., Dowson, D.: Ball Bearing Lubrication-The Elastohydrodynamics of Elliptical Contacts. Wiley, New York (1981)
28. Zavieh, A.H., Espallargas, N.: Effect of 4-point bending and normal load on the tribocorrosion-fatigue (multi-degradation) of stainless steels. Tribol. Int. (2016a). https://doi.org/10.1016/j.triboint.2016.03.016
29. Shirley, D.A.: High-resolution X-ray photoemission spectrum of the valance bands of gold. Phys. Rev. B (1972). https://doi.org/10.1103/PhysRevB.5.4709
30. Du, B., Johannsmann, D.: Operation of the quartz crystal microbalance in liquids: derivation of the elastic compliance of a film from the ratio of bandwidth shift and frequency shift. Langmuir (2004). https://doi.org/10.1021/la0359651
31. Nalam, P.C., Clasohm, J.N., Mashaghi, A., Spencer, N.D.: Macrotribological studies of poly(L-Iysine)-graft-poly(ethylene glycol) in aqueous glycerol mixtures. Tribol. Lett. (2010). https://doi.org/10.1007/s11249-009-9549-9
32. Acharya, B., Chestnut, M., Marek, A., Smirnov, A.I., Krim, J.: A combined QCM and AFM study exploring the nanoscale lubrication mechanism of silica nanoparticles in aqueous suspension. Tribol. Lett. (2017). https://doi.org/10.1007/s11249-017-0898-5
33. Zachariah, Z., Nalam, P.C., Ravindra, A., Ra, A., Mohanlal, A., Wang, K., Castillo, R.V., Espinoza-Marzal, R.M.: Correlation between the adsorption an the nanotribological performance of fatty acid-based organic friction modifiers on stainless steel. Tribol. Lett. (2020). https://doi.org/10.1007/s11249-019-1250-z
34. Fry, B.M., Moody, G., Spikes, H.A., Wong, J.S.S.: Adsorption of organic friction modifier additives. Langmuir (2020). https://doi.org/10.1021/acs.langmuir.9b03668
35. Zavieh, A., Espallargas, N.: The effect of friction modifiers on tribocorrosion and tribocorrosion-fatigue of austenitic stainless steel. Tribol. Int. (2017). https://doi.org/10.1016/j.triboint.2017.03.008
36. Willenbruch, R.D., Clayton, C.R., Oversluizen, M., Kim, D., Lu, Y.: An XPS and electrochemical study of the influence of molybdenum and nitrogen on the passivity of austenitic stainless steel. Corros. Sci. (1990). https://doi.org/10.1016/0010-938X(90)90106-F
37. Zavieh, A., Espallargas, N.: The role of surface chemistry and fatigue on tribocorrosion of austenitic stainless steel. Tribol. Int. (2016b). https://doi.org/10.1016/j.triboint.2016.07.020
38. Clayton, C.R.: A bipolar model of the passivity of stainless steel: the role of Mo addition. J Electrochem. Soc. (1986). https://doi.org/10.1149/1.2108451
39. Liu, Y., Shen, L.: From langmuir kinetics to first- and second-order rate equations for adsorption. Langmuir (2008). https://doi.org/10.1021/la801839b
40. Nalam, P.C., Pham, A., Veronica Castillo, R., Espinosa-Marzal, R.M.: Adsorption behavior and nanotribology of amine-based friction modifiers on steel surfaces. J. Phys. Chem. C (2019). https://doi.org/10.1021/acs.jpcc.9b02097